


Mapping the IMiD-dependent cereblon interactome using BioID-proximity labelling

Matteo Costacurta^{1,2}, Jarrod J. Sandow^{3,4}, Belinda Maher^{1,2}, Olivia Susanto^{1,2}, Stephin J. Vervoort³, Jennifer R. Devlin^{5,6}, Daniel Garama^{7,8}, Mark R. Condina^{9,10}, Joel R. Steele^{11,12}, Hossein V. Kahrood¹¹, Daniel Gough^{7,8}, Ricky W. Johnstone^{5,6} and Jake Shortt^{1,2,5,6} 

¹ Monash Haematology, Monash Health, Clayton, Australia

² Blood Cancer Therapeutics Laboratory, School of Clinical Sciences at Monash Health, Monash University, Clayton, Australia

³ The Walter and Eliza Hall Institute of Medical Research, Melbourne, Australia

⁴ Department of Medical Biology, The University of Melbourne, Parkville, Australia

⁵ Translational Haematology Program, Peter MacCallum Cancer Centre, Melbourne, Australia

⁶ Sir Peter MacCallum Department of Oncology, The University of Melbourne, Parkville, Australia

⁷ Centre for Cancer Research, Hudson Institute of Medical Research, Clayton, Australia

⁸ Department of Molecular and Translational Science, Monash University, Clayton, Australia

⁹ Mass Dynamics, Melbourne, Australia

¹⁰ Clinical & Health Sciences, University of South Australia, Adelaide, Australia

¹¹ Monash Proteomics and Metabolomics Platform, Monash Biomedicine Discovery Institute, Monash University, Clayton, Australia

¹² Monash Bioinformatics Platform, Monash Biomedicine Discovery Institute, Monash University, Clayton, Australia

Keywords

BioID2; bortezomib; cereblon; IMiDs; myosin

Correspondence

R. W. Johnstone, Translational Haematology Program, Peter MacCallum Cancer Centre, Melbourne, Vic. 3000, Australia

Tel: +6185597133

E-mail: ricky.johnstone@petermac.org

and

J. Shortt, Monash Haematology, Monash Health, 246 Clayton Rd, Clayton, Vic. 3168, Australia

Tel: +61385722884

E-mail: jake.shortt@monash.edu

Ricky W. Johnstone and Jake Shortt contributed equally to this article.

Immunomodulatory imide drugs (IMiDs) are central components of therapy for multiple myeloma (MM). IMiDs bind cereblon (CRBN), an adaptor for the CUL4-DDB1-RBX1 E3 ligase to change its substrate specificity and induce degradation of ‘neosubstrate’ transcription factors that are essential to MM cells. Mechanistic studies to date have largely focussed on mediators of therapeutic activity and insight into clinical IMiD toxicities is less developed. We adopted BioID2-dependent proximity labelling (BioID2-CRBN) to characterise the CRBN interactome in the presence and absence of various IMiDs and the proteasome inhibitor, bortezomib. We aimed to leverage this technology to further map CRBN interactions beyond what has been achieved by conventional proteomic techniques. In support of this approach, analysis of cells expressing BioID2-CRBN following IMiD treatment displayed biotinylation of known CRBN interactors and neosubstrates. We observed that bortezomib alone significantly modifies the CRBN interactome. Proximity labelling also suggested that IMiDs augment the interaction between CRBN and proteins that are not degraded, thus designating ‘neointeractors’ distinct from previously disclosed ‘neosubstrates’. Here we identify Non-Muscle Myosin Heavy Chain

Abbreviations

Bort, bortezomib; CAND1, cullin associated and neddylation dissociated 1; CCT3, chaperonin containing TCP1 subunit 3; CELMoDs, cereblon E3 ligase modulating drugs; CHORDC1, cysteine and histidine rich domain containing 1; CK1a, casein kinase 1 alpha; COP9, constitutive photomorphogenesis 9; COPS3/7A/7B, COP9 signalosome complex subunit 3/7A/7B; CRBN, cereblon; CRL4, cullin RING ligase 4; CUL4A/B, cullin 4A/B; DDB1, DNA damage binding protein 1; DVL1/2, dishevelled 1/2; eIF3C, elongation initiation factor 3C; G3BP1, G3BP stress granule assembly factor 1; HNRNP, heterogeneous nuclear ribonucleoprotein; HSP27/40/90/110, heat shock protein 27/40/70/90/110; Iber, iberdomide; IKZF1, Ikaros family zinc finger 1; IKZF3, Aiolos, Ikaros family zinc finger 3; IL2, interleukin 2; IMiDs, immunomodulatory imide drugs; IRF4, interferon regulatory factor 4; Len, lenalidomide; LFA-1, lymphocyte function-associated antigen 1; MM, multiple myeloma; MS, mass spectrometry; MYC, myelocytomatosis; MYH9, non-muscle myosin heavy chain IIA; NKG2D, natural killer group 2D receptor; Pom, pomalidomide; PRDX4, peroxiredoxin 4; PROTACs, proteolysis targeting chimeras; RBX1, RING box protein 1; TXNL1, thioredoxin-like protein 1; ZFP91, zinc finger protein 91.

(Received 3 December 2023, revised 17 April 2024, accepted 24 May 2024)

doi:10.1111/febs.17196

IIA (MYH9) as a putative CRBN neointeractor that may contribute to the haematological toxicity of IMiDs. These studies provide proof of concept for proximity labelling technologies in the mechanistic profiling of IMiDs and related E3-ligase-modulating drugs.

Introduction

Immunomodulatory imide drugs (IMiDs; e.g., lenalidomide and pomalidomide) are an important backbone of multiple myeloma (MM) therapy [1]. However, patients often develop IMiD-resistant MM and may experience clinical toxicities, including peripheral neuropathy, myelosuppression and thrombosis. Greater understanding of mechanistic activity, including the mediators of toxicity, may help further optimise IMiD therapy to improve patient outcomes [2–7].

The IMiDs are known to engage Cereblon (CRBN), an adaptor for Cullin RING E3 Ligase 4 (CRL4), redirecting its substrate specificity towards the neosubstrates Ikaros (IKZF1) and Aiolos (IKZF3), resulting in their proteasomal degradation [8,9]. Functional studies have revealed that the ubiquitinating activity of CRL4^{CRBN} is also dependent on the Constitutive Photomorphogenesis Signalosome 9 (COP9 signalosome) and its subunits which regulate NEDDylation of Cullin scaffolds, Cullin Associated and Neddylated Dissociated 1 (CAND1), and other ubiquitin ligases [10–16]. In MM, IKZF1/3 degradation leads to downregulation of the Interferon Regulatory Factor 4 (IRF4)-MYC transcriptional axis and plasma cell death [8]. Degradation of these transcription factors also de-represses Interleukin-2 (*IL2*) expression to augment T-cell activity [8]. Recent work has demonstrated that CRBN regulates oxidative stress, protein folding (as a HSP90 co-chaperone), and that IMiDs also modulate these processes, potentially via mechanisms that are independent from their effects on neosubstrate proteins [17–19]. New generation IMiDs (or CELMoDs – Cereblon E3 Ligase Modulating Drugs) have now been rationally designed for improved potency and these demonstrate diversity of neosubstrate repertoires and differential mechanistic properties [20]. These findings suggest that IMiDs act at multiple levels, and their biology remains incompletely mapped.

To gain deeper insight into mechanisms of IMiD action, we aimed to map the CRBN interactome in the presence and absence of IMiDs and proteasomal inhibition. To achieve this, we utilised BioID2, a ligase that biotinylates proximal lysine residues in the presence of free biotin [21–23]. We hypothesised that generating a BioID2-CRBN fusion protein would provide

BioID2 with increased specificity for CRBN interactors and substrates, as they would now be proximal to BioID2. A separate group recently utilised an analogous approach, where fusion of CRBN to TurboID or AirID identified known CRBN-IMiD neosubstrates (including IKZF1, IKZF3, CK1 α , ZFP91) via proximity-dependent biotinylation [24]. Here, we have evaluated protein biotinylation in the context of the IMiDs (lenalidomide, pomalidomide) and the CELMoD, iberdomide and validated our approach by the identification of canonical CRBN interactors (e.g., CUL4A/B, COPS7A/B, COPS3) and IMiD-CRBN neosubstrates (e.g., IKZF1 and CK1 α).

In addition to detecting known CRBN interactors and IMiD-CRBN substrates, we identified non-muscle myosin heavy chain IIA (MYH9) as a novel CRBN interactor. We prioritised MYH9 for further validation, given its known importance as a cytoskeletal protein implicated in cell morphology, migration, platelet biogenesis and aggregation [25–27]. Here we demonstrate that IMiDs augment the interaction between CRBN and MYH9. Unlike previously identified IMiD-CRBN neosubstrates, our data indicate that MYH9 is a protein that may be ubiquitinated, but not degraded, following IMiD treatment. We postulate that the IMiD-augmented interaction between CRBN and MYH9 might contribute to cellular and clinical phenotypes, including cell motility, platelet function and thrombogenicity. In addition, we show that stabilisation of proteins following inhibition of proteasomal activity may significantly change the CRBN interactome. Our work further supports proximity-labelling approaches as a methodology for identifying endogenous and drug-dependent CRBN interactors which could be broadly utilised across the growing pool of IMiD, CELMoD and PROTAC chemotypes [20,28].

Results

BioID2-CRBN biotinylates known endogenous CRBN interactors

HEK293T cells were transiently transfected with a vector expressing either myc-tagged BioID2 (mycBioID2)

or BioID2-CRBN (mycBioID2-CRBN, with BioID2 fused at CRBN N terminus domain through a 3xGlycine linker), and expression of ectopic proteins was confirmed by western blot (Fig. 1A). These cells were cultured for 24 h with 50 μ M biotin, followed by purification of biotinylated proteins with streptavidin-agarose and mass spectrometry (MS; Fig. 1B; [Supporting Information](#)). As expected, this approach identified CRBN as the most enriched biotinylated protein, while previously identified CRBN interactors COPS7A, COPS7B, COPS3, CUL4A and CUL4B [11,14,29] (Fig. 1C,D) were also significantly enriched in the biotinylated fraction. Based on protein–protein interaction analysis via STRING, we defined proteins that did not connect to CRBN as putative novel CRBN interactors (Fig. 1E). Gene ontology analysis revealed that these known, and potentially novel interactors together primarily promote DNA repair and protein metabolism and turnover, whereas biotin-binding proteins are likely an artefact of the technology (Fig. 1E,F; [Supporting Information](#)). Thus, mycBioID2-CRBN biotinylates known CRBN interactors and this methodology identifies putatively novel CRBN interactors that are not readily identified by conventional MS-techniques.

BioID2-CRBN induces biotinylation of known CRBN neosubstrates

To test whether mycBioID2-CRBN could biotinylate IMiD-CRBN neosubstrates, we transduced OPM2 MM cells to stably express mycBioID2-CRBN (OPM2-BioID2-CRBN cells). Western blot confirmed expression of BioID2-CRBN in OPM2-BioID2-CRBN cells as compared to OPM2-BioID2, which did not express BioID2-CRBN, but only BioID2 (Fig. 2A). We noted a dominant secondary band above the 25 kD BioID2 band that was also immunoreactive with myc-tag antibody and was not evident in the previous HEK293T experiment of uncertain significance. We then treated OPM2-BioID2-CRBN cells with DMSO, Lenalidomide (Len), pomalidomide (Pom) or iberdomide (Iber) in the presence and absence of bortezomib (Bort), while supplementing the culture medium with biotin (Fig. 2B). Bort co-treatment was included to prevent proteasomal degradation of IMiD-CRBN neosubstrates and to allow their enrichment with streptavidin-agarose prior to mass spectrometry analysis (see [Supporting Information](#)). Differential protein enrichment analysis confirmed that the BioID2-CRBN fusion protein specifically biotinylates known CRBN interactors (Fig. 2C). Seven hundred and nine proteins were purified as biotinylated

species. Analysis of variance defined a significant change in biotinylation across the different treatment conditions in 102 proteins (adj. *P*-value < 0.05) (Fig. 2C). IMiD-CRBN neosubstrates identified in this experiment included IKZF1 and CK1 α (CSNK1A1; CSNK1A1L) (Fig. 2C). IKZF1 was significantly more biotinylated in cells co-treated with Bort and IMiDs – Len, Pom and Iber for IKZF1, Len and Iber for CK1 α – as compared to cells treated with their respective IMiD-only condition, confirming that BioID2-CRBN biotinylates these canonical CRBN neosubstrates in the presence of an IMiD (Fig. 2D). Interestingly, Iber is not a CK1 α degrader [30], nor is Pom [31], however biotinylation of CK1 α is still observed in the presence of Iber and Pom, indicating that an interaction between CRBN and CK1 α occurs in the presence of these IMiDs, but does not result in degradation (Fig. 2D). We then overlapped the 47 proteins that were more biotinylated by BioID2-CRBN (as compared to BioID2 alone) in HEK293T cells and the 709 proteins that were purified in OPM2-BioID2-CRBN cells, with 37 overlaps identified (Fig. 2E). Alongside canonical CRBN interactors, proteins implicated in the ubiquitination machinery, in the NEDDylation process, and biotin-binding proteins, were detected as biotinylated species. Enzymes that regulate oxidative stress (thioredoxin like protein 1 – TXNL1, and peroxiredoxin 4 – PRDX4) were also biotinylated, suggesting that CRBN and IMiDs may have a role in directly regulating this process, as previously described (Fig. 2F) [17]. Together, these data suggest that proximity labelling facilitates the detection of known and potentially novel endogenous CRBN interactors and E3 ligase substrates, including those dependent on or augmented by the presence of an IMiD.

BioID2-CRBN demonstrates overlapping specificity between distinct IMiD chemotypes

Previous studies have already mapped the interactome and neosubstrate repertoire of thalidomide and the first generation of IMiDs (i.e., lenalidomide and pomalidomide) [20]. There is now an increasing array of new-generation CELMoDs based on enhanced CRBN-mediated target protein degradation, including iberdomide which is active in IMiD-resistant MM [32]. As the therapeutic landscape of CRBN-interacting small molecules becomes more diverse, sensitive methodologies for determining overlapping and divergent neosubstrate and neointeracting proteins may further assist in drug optimisation and mechanistic understanding of activity and toxicity profiles [20].

OPM2-BioID2-CRBN data was further analysed. As observed in the heatmap of Fig. 2C, each of the three IMiD chemotypes increases the biotinylation of diverse

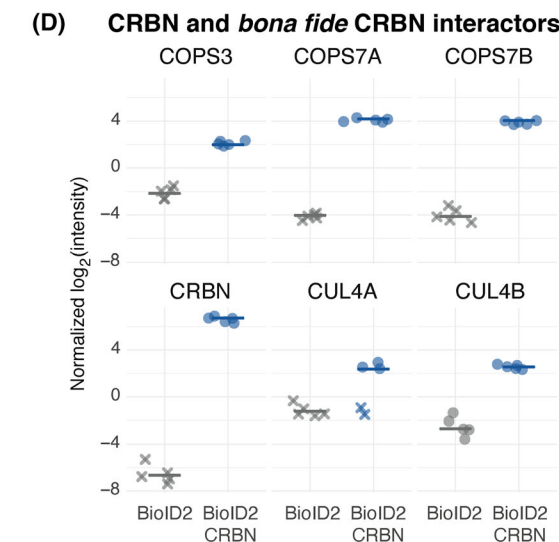


Fig. 1. Transient expression of BioID2-CRBN induces biotinylation of *bona fide* CRBN interactors. (A) Western blots (WB) showing expression of CRBN (top WB) and myc-tag (bottom WB) in HEK293T cells transfected with either *pBABE-mycBioID2-puroR* (mycBioID2) or *pBABE-mycBioID2-CRBN-puroR* (mycBioID2-CRBN) as compared to HEK293T cells transfected with *pBABE-puroR* empty vector. Actin is used as a loading control for myc-tag expression. CRBN and myc-tag were probed for in two separate WB obtained from the same samples. Endogenous CRBN expression is used as a loading control for the CRBN WB, whilst actin is used as a loading control for the myc-tag WB. (B) Schematic representation of the experimental design for proteomics analysis of biotinylated proteins in HEK293T cells expressing either mycBioID2 or mycBioID2-CRBN. Cells were transiently transfected with either *pBABE-mycBioID2-puroR* (mycBioID2) or *pBABE-mycBioID2-CRBN-puroR* (mycBioID2-CRBN), incubated for 48 h, then lysed in RIPA buffer. Streptavidin-agarose resins were then employed to purify the biotinylated protein fraction. Purified fractions from each sample were therefore digested with trypsin overnight and subsequently processed for mass spectrometry with label-free quantification (LFQ). Five technical replicates were used for the experiment. (C) Volcano plot displaying differential protein biotinylation in HEK293T cells expressing either mycBioID2 or mycBioID2-CRBN. Blue dots represent proteins that are significantly more biotinylated when cells express mycBioID2-CRBN, as compared to cells expressing mycBioID2 (adj. *P*-value < 0.05). (D) Dot plots showing normalised log₂ of protein intensities for COPS3, COPS7A, COPS7B, CRBN, CUL4A and CUL4B in each technical replicate. Horizontal bars represent the median log₂ intensity value. Circles represent detected intensity values; crosses represent imputed values. (E) Protein–protein interaction network (STRING) and (F) Gene ontology analysis (ToppFun) of proteins that are significantly more biotinylated when cells express mycBioID2-CRBN, as compared to cells expressing mycBioID2 (adj. *P*-value < 0.05).

sets of proteins via BioID2-CRBN. In an attempt to restrict the specificity of our assay to true novel interactors, we selected proteins that were significantly more biotinylated with IMiDs or Bort-IMiD. Amongst these, we filtered out those that were more biotinylated in the presence of Bort to ensure that increased biotinylation in Bort-IMiD conditions is not induced by the presence of Bort alone (Fig. 2G). Within this subset of biotinylated proteins, some were chemotype-specific, while others were biotinylated in the presence of any IMiD. Len and Pom induced biotinylation of five and three proteins, respectively, while Iber induced biotinylation of 10 proteins. The two proteins biotinylated in the presence of all the three IMiDs were IKZF1 and MYH9 (Fig. 2H). This observation suggests that Iber broadens CRBN's pool of interactors. The biological consequence of these putative interactions is not completely understood. However, this result suggests that proximity labelling may help dissect how the CRBN interactome changes when CRBN is bound to different IMiD or CELMoD chemotypes.

CRBN interactome is modulated by proteasome inhibition

As Bort inhibits proteolytic activity of the proteasome and CRBN has been described to regulate protein folding by binding with HSP90, we also hypothesised that treatment with this agent may modulate CRBN pool of interactors (i.e., in the absence of an IMiD). Interestingly, analysis of the correlation between samples with unsupervised clustering showed that the presence or absence of Bort defines the two largest clusters in the dataset (Fig. 3A), indicating that Bort strongly influences the pool of CRBN interactors. Bort

treatment induced increased or decreased biotinylation of 47 proteins (Fig. 3B,C). Dishevelled proteins –1 and –2 (DVL1, DVL2) were those with the most significant decrease in biotinylation in the presence of Bort, indicating that CRBN interacts with DVL proteins and that treatment with Bort disrupts this interaction. In contrast, Bort induced biotinylation of the known endogenous CRBN substrate HSP70 (HSPA1A/B) [33], and other chaperones, such as HSP40 (DNAJB1), HSP27 (HSPB1), HSP10 (HSPE1), HSP110 (HSPH1), and HSP90 co-chaperones Morgana (CHORDC1) [34], and CCT3 [35], raising the hypothesis that CRBN regulates the activity of multiple chaperone proteins (Fig. 3B,C). In addition, we observed significantly increased biotinylation of stress granule components G3BP1, HNRNP proteins, eIF3C, suggesting that CRBN might participate in the formation of stress granules during Bort treatment [36–38]. These observations, taken together, suggest that Bort itself may modify the CRBN interactome and thus modulate CRBN activity as E3 ligase and chaperone.

IMiD treatment augments the interaction between CRBN and MYH9

To identify proteins that may be engaged by CRBN in the presence of an IMiD but not subsequently degraded, we performed differential protein expression analysis of biotinylated proteins that are enriched with IMiDs only- versus vehicle-treated cells. The only protein meeting the statistical threshold (adj. *P*-value < 0.05) that was differentially biotinylated between these conditions was non-muscle myosin heavy chain IIA (MYH9). This protein was significantly more biotinylated by treatment with both

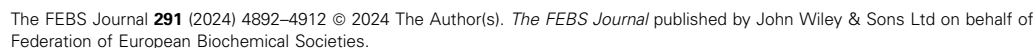


Fig. 2. Profiling biotinylation demonstrates differential potency and specificity of IMiD chemotypes and allows prediction of potential novel neosubstrates. (A) Western blot showing expression of myc-tag at 1 and 5 min of exposure in OPM2 cells transduced with either mycBioID2 or mycBioID2-CRBN. Tubulin expression is used as a loading control. Experiment representative of three independent experiments. (B) Schematic representation of the experimental design for proteomics analysis of biotinylated proteins in OPM2 cells expressing either mycBioID2 or mycBioID2-CRBN. Cells were treated overnight (16 h) with DMSO, 10 μ M Lenalidomide (Len), 2 μ M Pomalidomide (Pom), 2 μ M Ixerdomide (Iber), 10 nM Bortezomib (Bort) or a combination of both Bort and each IMiD. Cells were then lysed in RIPA buffer. Streptavidin-agarose resins were then employed to purify the biotinylated protein fraction. Purified fractions from each sample were therefore digested with trypsin overnight and subsequently processed for mass spectrometry with label-free quantification (LFQ). Five technical replicates were used for each condition of the experiment. (C) Heatmap showing z-scores of median normalised log₂ intensity of biotinylated proteins across all conditions that are significant for adj. *P*-value < 0.05 (analysis of variance) and that are differentially expressed across the various treatment conditions. (D) Dot plots showing normalised log₂ intensities of IKZF1 and CK1 α in each technical replicate. Horizontal bars represent the median log₂ intensity value. Circles represent real values; crosses represent imputed values. (E) Venn diagram showing overlap between proteins that are differentially biotinylated in HEK293T cells (expressing BioID2-CRBN) as compared to those expressing mycBioID2) and those that are found biotinylated in OPM2 cells (expressing BioID2-CRBN), with a cut-off at adj. *P*-value < 0.05. (F) Protein–protein interaction network of these 37 overlapping genes (known and novel putative interactors) generated using STRING-db. (G) Heatmap showing z-scores of median normalised log₂ intensity of the subset of proteins significantly more biotinylated by BioID2-CRBN in the presence of an IMiD (adj. *P*-value < 0.05), corrected for the effect of Bort. Only proteins that were biotinylated by any Bort-IMiD more than Bort only of at least 1 standard deviation were included. (H) Binary heatmap showing proteins that are significantly more biotinylated by BioID2-CRBN following treatment with a specific IMiD. A black square defines the presence of an interaction by the criteria described in (E), a blank square defines an interaction is either absent or does not meet the above criteria.

IMiDs and Iber (Fig. 4A,B). We observed that MYH9 demonstrates basal biotinylation even in the absence of an IMiD, suggesting that CRBN has an endogenous interaction with MYH9 under physiological conditions and that IMiD exposure further augments this (Fig. 4B). To further validate the increase in MYH9 biotinylation upon IMiD treatment, enrichment of biotinylated proteins was performed on Len-treated HEK293T cells transiently expressing BioID2-CRBN (Fig. 4C). Consistent with MS data (Fig. 4A), Len treatment, but not single-agent Bort, increased the biotinylation of MYH9 (Fig. 4C, lower panel), while the total amount of MYH9 in the cell was not affected by Len exposure (Fig. 4C, upper panel). This observation was also demonstrated in HEK293T cells expressing BioID2-CRBN, with each of the IMiD chemotypes (Len, Pom or Iber; Fig. 4D). Additionally, we sought to explore whether IMiD treatment induced any changes in the amount or cellular distribution of MYH9 via immunofluorescence using IKZF1 as a positive control (Fig. 5). We observed that, while IKZF1 intensity was reduced in parental OPM2 cells receiving Len treatment, MYH9 levels were unchanged. Moreover, neither MYH9 intracellular distribution pattern nor cell morphology were affected by exposure to Len. To cross-validate the occurrence of an increased interaction between CRBN and MYH9 that is IMiD-dependent, we reviewed published data obtained utilising AirID-CRBN as a biotin proximity-labelling tool in IMiD-treated MM.1S, HEK293T, HuH7 and IMR32 cells [24] (Fig. 6A). Consistent with our own

data, MYH9 peptides demonstrated a significant increase in biotinylation, particularly in the presence of Len and Pom.

IMiDs induce ubiquitination of MYH9 via CRBN

Having identified an interaction between CRBN and MYH9 using BioID2-modified CRBN, we next sought to identify if this interaction is evident in the context of endogenous CRBN protein. CRBN is known to ubiquitinate proteins which do not undergo subsequent proteasomal degradation so we posited that CRBN may ubiquitinate MYH9 with potential functional consequences. Using previously published ubiquitin-MS/MS datasets of IMiD-treated MM cells [8] we sought to determine if MYH9 was ubiquitinated by CRBN in the presence of an IMiD. Analysis of differentially ubiquitinated peptides via detection of diglycine modifications on lysine residues was performed (Fig. 6B, see [Supporting Information](#)). As expected, the most significant ubiquitinated peptides belong to IKZF1, IKZF3 and CK1 α . Although ubiquitinated, these peptides showed low abundance in Len-treated cells as they had not been ‘protected’ by co-treatment with a proteasome inhibitor. Conversely, differentially ubiquitinated peptides with stable or increased abundance were evident, including MYH9 peptides. The K821 residue, a lysine of the MYH9 neck region, was significantly more ubiquitinated in the presence of Len, as compared to DMSO vehicle treatment (adj. *P*-value < 0.05 (Fig. 6B)). This

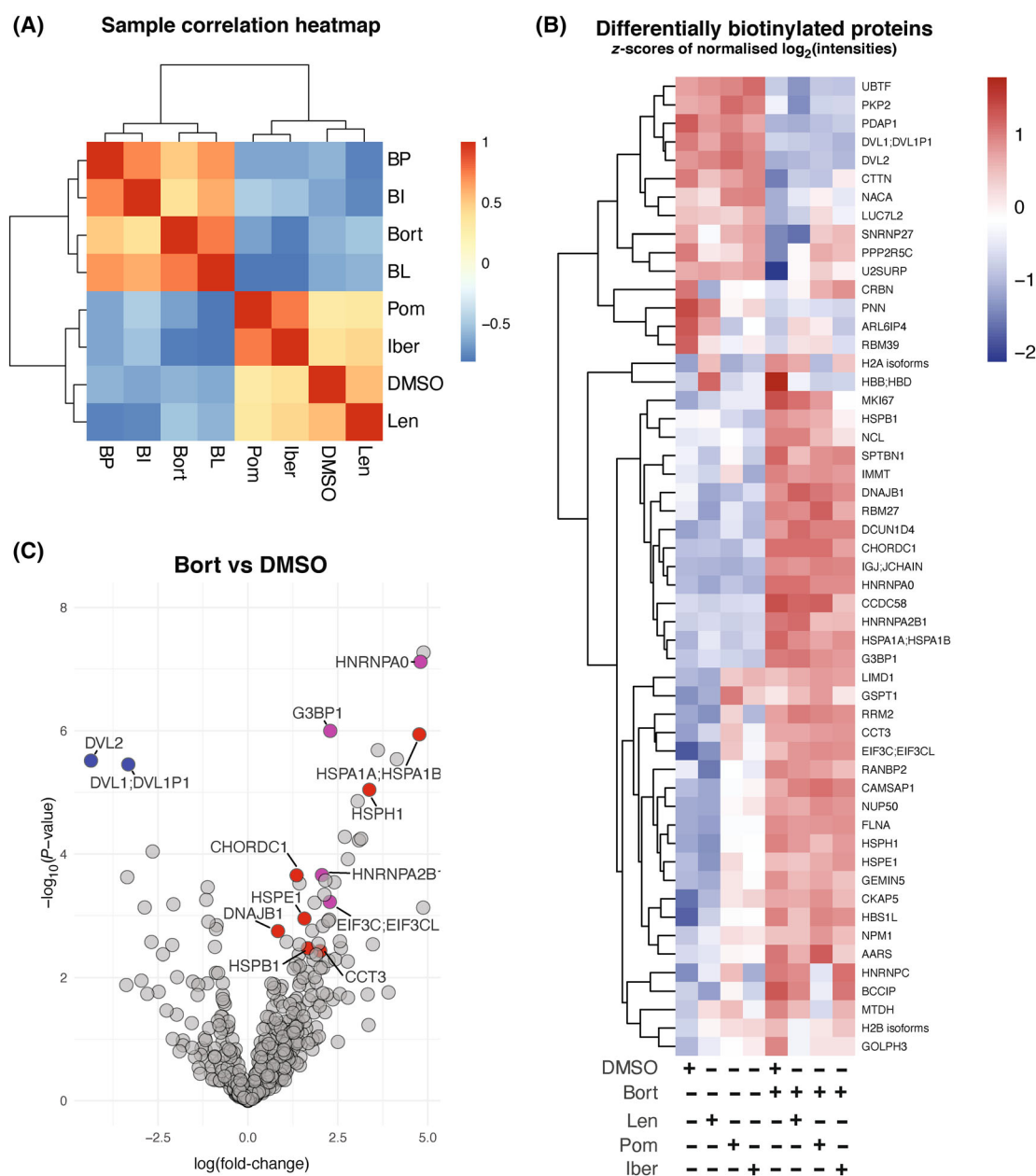


Fig. 3. Bortezomib significantly perturbs the CRBN interactome. (A) Heatmap showing correlation between samples treated with DMSO, 10 nM bortezomib (Bort), 10 μ M lenalidomide (Len), 2 μ M pomalidomide (Pom), 2 μ M iberdomide (Iber), and a combination of Bort and Len (BL), Bort and Pom (BP), and Bort and Iber (BI). (B) Heatmap showing proteins that are significantly more or less biotinylated by BioID2-CRBN in the presence of Bort (adj. P -value < 0.05). (C) Volcano plot displaying differential biotinylation of proteins in OPM2 cells expressing BioID2-CRBN that are treated with each Bort as compared to DMSO. Red dots represent proteins that are significant for adj. P -value < 0.05 and are more biotinylated in the presence of Bort. In blue, DVL1/2 proteins, in purple, proteins implicated in stress granule formation, in red, proteins involved in protein homeostasis.

supports data obtained using BioID2 and further indicates an occurring interaction between endogenous CRBN and MYH9 that is augmented by Len and results in ubiquitination of MYH9 via engagement of CRL4^{CRBN}.

Discussion

With this work, we generated a fusion protein between CRBN and BioID2, with the aim of detecting proximal CRBN interactors and substrates with high

sensitivity and specificity. While the success of antibody co-immunoprecipitation is determined by the strength of the lysis technique and washing conditions, BioID2 proximity labelling allows the use of more stringent lysis conditions to increase the sensitivity and specificity of the purification process [21–23]. Accordingly, BioID2 can identify weaker protein–protein interactions or those occurring transiently. We opted not to generate a C-terminus fused CRBN-BioID2 counterpart as we hypothesised that adding a large protein adduct near the thalidomide binding domain could interfere with CRBN substrate engagement [39]. Additionally, we adopted a short linker between BioID2 and CRBN (Gly-Gly-Gly), possibly limiting the movement of the biotinylation. Further studies could explore how the biotinylation changes when BioID2 is fused to the C-terminus of CRBN or is fused to CRBN with a longer and more flexible linker.

The fusion of BioID2 with CRBN allowed biotinylation and purification of known CRBN interactors (CUL4A/B and members of the COP9 signalosome), supposedly of those that are spatially closer to CRBN N-terminus domain, and of many other putative interactors. Based on this assumption, it could be hypothesised that CRBN is spatially closer to COPS7A/B and COPS3 than the other COP9 signalosome subunits. This may explain the absence of DDB1 in our biotinylated fraction, as DDB1 interacts with the central helical bundle domain of CRBN and not with its N-terminal domain [39]. On the other hand, identification of CUL4A and B may be explained by the well-described CUL4 rotational movement during target ubiquitination, which could reduce the distance between CRBN and CUL4 itself, resulting in CUL4 biotinylation [39]. Given the potential sensitivity of BioID2 to detect proximal proteins, it was unexpected that RBX1 was not enriched in pulldown experiments. This may reflect low RBX1 peptide abundance in the experimental conditions.

IMiD treatment induced biotinylation and stabilisation of *bona fide* neosubstrates IKZF1 and CK1 α . Curiously we were not able to stabilise IKZF3, possibly indicating suboptimal biotinylation due to conformation of the degradation complex, lack of exposure of lysine residues by IKZF3 as compared to IKZF1 in BioID2 proximity, or other technical limitation of the mass spectrometry assay (e.g., lack of appropriate peptide coverage, inadequate amount of input or purified lysate). Other putative IMiD interactors were identified by subtracting the effect of Bort from that of IMiDs, and these displayed chemotype-specific selectivity. When using proximity labelling to detect interactors of a specific protein, the pool of putative interactors

could significantly change with different biotinylators (e.g., AirID, TurboID), or if the biotinylation is fused to CRBN with linkers of different length, or also if this is linked to the C-terminus of CRBN, rather than the N-terminus.

The presence of bortezomib was able to cause significant changes in the fraction of proteins that are biotinylated by BioID2-CRBN. Dishevelled proteins were biotinylated in the absence of Bort, and not detected with Bort treatment, suggesting that CRBN interacts with DVL1/2 and participates in regulating the Wnt/ β -catenin pathway, but also that Bort may disrupt this interaction. Further interrogation of the biological significance of this interaction could reveal undisclosed mechanisms by which IMiDs and Bort modulate the bone marrow microenvironment via the Wnt/B-catenin pathway.

Proteins implicated in the oxidative stress regulation and chaperone proteins were more biotinylated in the presence of Bort, indicating that CRBN might interact with these proteins and regulate these processes, especially when significant perturbation of the proteome is induced by proteasome inhibition. This observation provides additional evidence to recent findings on Len treatment being able to induce oxidative stress in MM cells [17] and on CRBN being a co-chaperone of HSP90, suggesting that CRBN might regulate the activity of additional chaperone proteins [19]. Finally, as increased biotinylation of proteins implicated in the formation of stress granules with Bort treatment, and proteasome inhibition causes formation of stress granules [36,38], we posit that CRBN activity might also regulate the response to proteasome inhibitors.

Increased biotinylation of MYH9 in the presence of an IMiD was found to be the most consistent across all IMiD conditions, making it the best ‘hit’ in our functional screen. This interaction was also evident in the data of Yamanaka *et al.* [24], who adopted an analogous approach using different bacterial biotin ligases (TurboID and AirID), providing orthogonal validation of MYH9 as potential CRBN interactor/substrate [24]. However, this group did not seek to validate the MYH9-CRBN interaction. Here we provide low-throughput validation, showing that MYH9 is biotinylated by BioID2-CRBN in the presence of an IMiD. Based on our data, however, MYH9 is not a degraded neosubstrate as it does not decrease in the presence of an IMiD and is not stabilised by proteasome inhibition. It was interesting to note a similar chemotype-dependent phenotype for CK1 α , which was biotinylated by Len, Pom and Iber but is only known to be degraded in response to Len. Others have

reported that MYH9 may be degraded after ubiquitination by ENKUR in complex with the E3 ligase FBXW7 [40]. Autophagy has also been linked to

regulation of MYH9 levels [41]. Given the multifaceted effects of ubiquitination in regulating protein levels, localisation and functions [42], CRBN-mediated

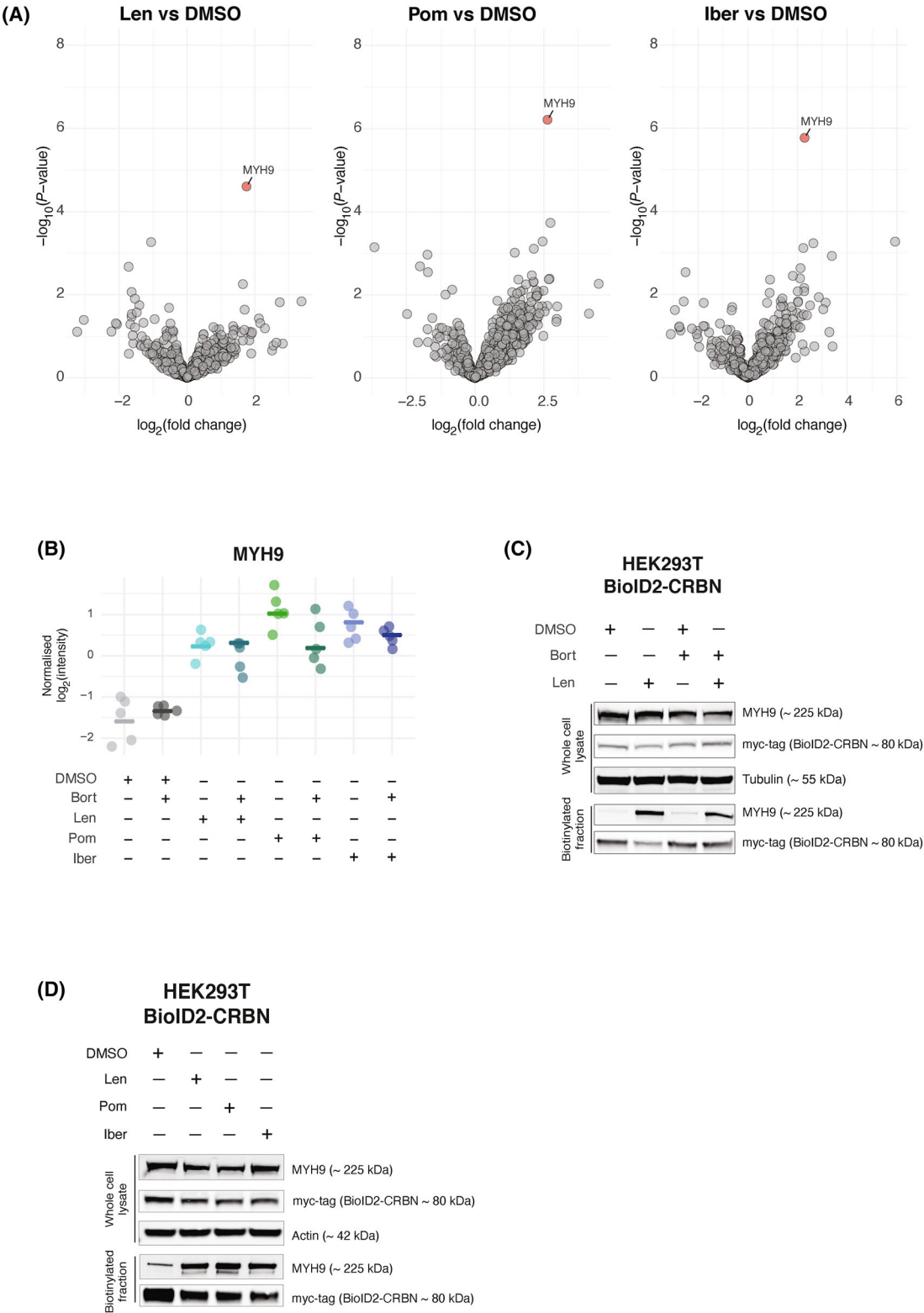


Fig. 4. MYH9 is a CRBN interactor. (A) Volcano plots displaying differential biotinylation of proteins in OPM2 cells expressing BioID2-CRBN that are treated with each IMiD as compared to DMSO. Red dots represent proteins that are significant for adj. *P*-value < 0.05 and are more biotinylated in the presence of an IMiD. (B) Dot plots showing normalised log₂ intensities of MYH9 in each technical replicate. Horizontal bars represent the median log₂ intensity value. (C) Western blot of HEK293T cells transiently transfected with *pBABE-mycBioID2-CRBN-puroR* and treated with DMSO, 10 µM Len, 10 nM Bort or BL for 16 h. Expression of MYH9 and myc-tag (for mycBioID2-CRBN detection) in the whole cell lysate is shown together with the expression of the same proteins in the purified fraction containing biotinylated proteins. In the whole cell lysate, expression of tubulin is used as a loading control. The western blot is representative of three independent experiments. (D) Western blot of HEK293T cells transiently transfected with *pBABE-mycBioID2-CRBN-puroR* and treated with DMSO, 10 µM Len, 2 µM Pom or 2 µM Iber for 24 h. Expression of MYH9 and myc-tag (for mycBioID2-CRBN detection) in the whole cell lysate is shown together with the expression of the same proteins in the purified fraction containing biotinylated proteins. In the whole cell lysate, expression of actin is used as a loading control. The western blot is representative of three independent experiments.

MYH9 ubiquitination may have no phenotype or support the fine-tuning of actin-myosin dynamics.

MYH9 is implicated in multiple biological processes, including cell migration and adhesion to the extracellular matrix, cell morphology, and also platelet maturation and function [25,27]. Several single MYH9 point mutations are known to cause platelet dysfunction and have been classified into a group of diseases called MYH9-related platelet disorders causing thrombocytopenia [26,43–45]. In addition to causing thrombocytopenia, IMiD treatment increases the risk of venous thrombosis [46]. Somewhat paradoxically, certain MYH9-related platelet disorders are also associated with thrombotic risk [47]. IMiD-induced aromatase degradation is reported to impair platelet maturation [48]. The prothrombotic state induced by IMiDs may be explained by promyelocyte expansion and increased expression of cathepsin G [49]. We have not validated whether the interaction between CRBN and MYH9 also contributes to platelet maturation and/or perturbs platelet aggregation dynamics. However, it can be hypothesised that CRBN regulates platelet dynamics via interaction with MYH9 and that IMiDs could alter thrombopoiesis and platelet aggregation. Focussed mapping of post-translational modifications of MYH9 following IMiD treatment may provide insight into potential functional consequences, particularly if residues known to be mutated in MYH9 disorders proximal to the ‘neck’ region are modified concurrently to K821.

IMiD treatment induces cellular stress fibre formation, a process involving the assembly of actomyosin filaments in Swiss 3T3 cells [50]. CRBN is reported to regulate actin activity in natural killer (NK) cells [51,52] where rearrangement of the cortical actin mesh is induced by IMiDs in the presence of additional stimuli (such as CXCL12 [51], anti-CD16 antibodies, LFA-1 and NKG2D co-ligation, rituximab [52]). This phenotype is CRBN and Cullin NEDDylation dependent [51], indicating a relevant role for the CRL4^{CRBN} complex in cell migration and NK cell activation. This

opens the possibility for a role of myosin (MYH9) lysine ubiquitination in the functional consequences of CRBN modulation on stress granule formation, cell migration and NK cell activation.

In conclusion, this work proposes an alternative methodology to define E3 ligase interactomes using an affinity-based methodology that may overcome some of the limitations of antibody-based pull-down techniques. The approach appears tractable across different cell types and IMiD chemotypes, providing an opportunity to identify potentially clinically relevant CRBN-interactors.

Materials and methods

Cell lines and cell culture media

OPM2 cells (DSMZ, RRID: CVCL_1625) were cultured in RPMI-1640 medium containing GlutaMAX (Gibco, ThermoFisher Scientific, Waltham, MA, USA) supplemented with 10% FBS (Bovogen Biologicals, Keilor East, Victoria, Australia), were split twice a week and grown in 5% CO₂ at 37 °C. HEK293T (RRID: CVCL_0063) were from Prof. Kaylene Simpson (Functional Genomics Facility, Peter MacCallum Cancer Centre, Melbourne, Victoria, Australia). HEK293T cells were cultured in DMEM containing GlutaMAX (Gibco) supplemented with 10% FBS, were split three times a week and grown in 10% CO₂ at 37 °C. OPM2 cell fidelity was confirmed by short tandem repeat profiling and cells were confirmed to be *Mycoplasma* infection-free before use. For biotinylation experiments, including western blot analysis and proteomics studies, on biotinylated proteins in OPM2 cells expressing BioID2 or BioID2-CRBN, biotin-free RPMI-1640 medium was utilised (Cell Culture Technologies, Gravesano, Switzerland) and was supplemented with 10 mM GlutaMAX and dialysed FBS. For the same experiments in HEK293T cells expressing BioID2 or BioID2-CRBN, standard DMEM + GlutaMAX was employed and it was supplemented with dialysed FBS. To perform FBS dialysis, 25 cm of Snake-Skin dialysis tube (ThermoFisher Scientific, Waltham, MA, USA) were filled with FBS, sealed, and immersed for 72 h

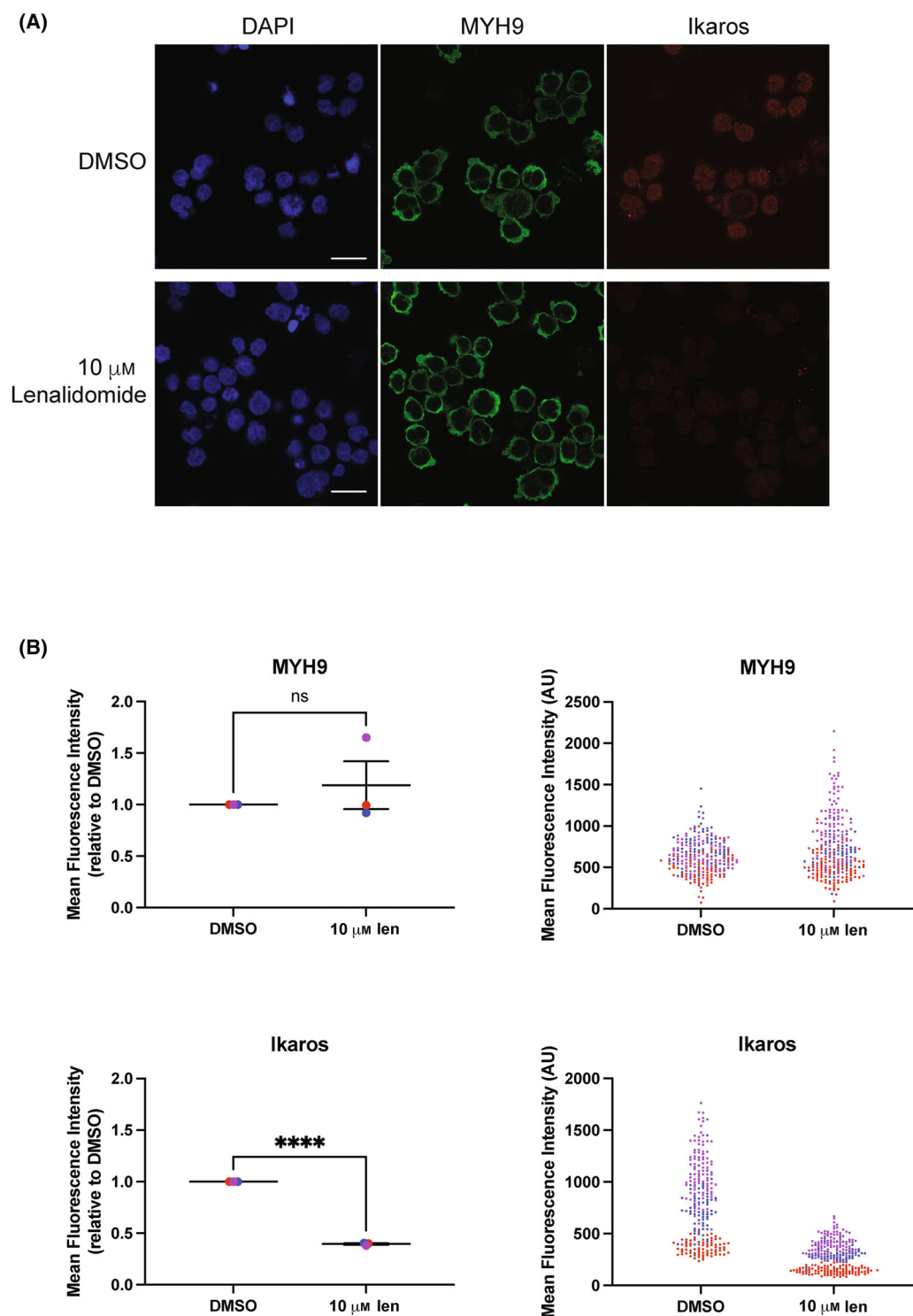


Fig. 5. MYH9 staining in OPM2 cells treated with lenalidomide. (A) Representative confocal images of OPM2 cells stained for DAPI (blue), MYH9 (green) and Ikaros (red), comparing DMSO-treated cells (top row) with those treated for 24 h with 10 μ M lenalidomide (bottom row). Scale bar represents 20 μ m. (B) Quantification of mean fluorescence intensity (MFI) of OPM2 cells, measuring either MYH9 (top row) or Ikaros (bottom row) fluorescence. (Left) Average MFI relative to DMSO for each independent experiment (**** $P < 0.0001$, t -test, error bars represent the standard error of the mean); (right) individual cell MFIs showing overall range, with each independent experiment coloured separately. Data is representative of three independent experiments.

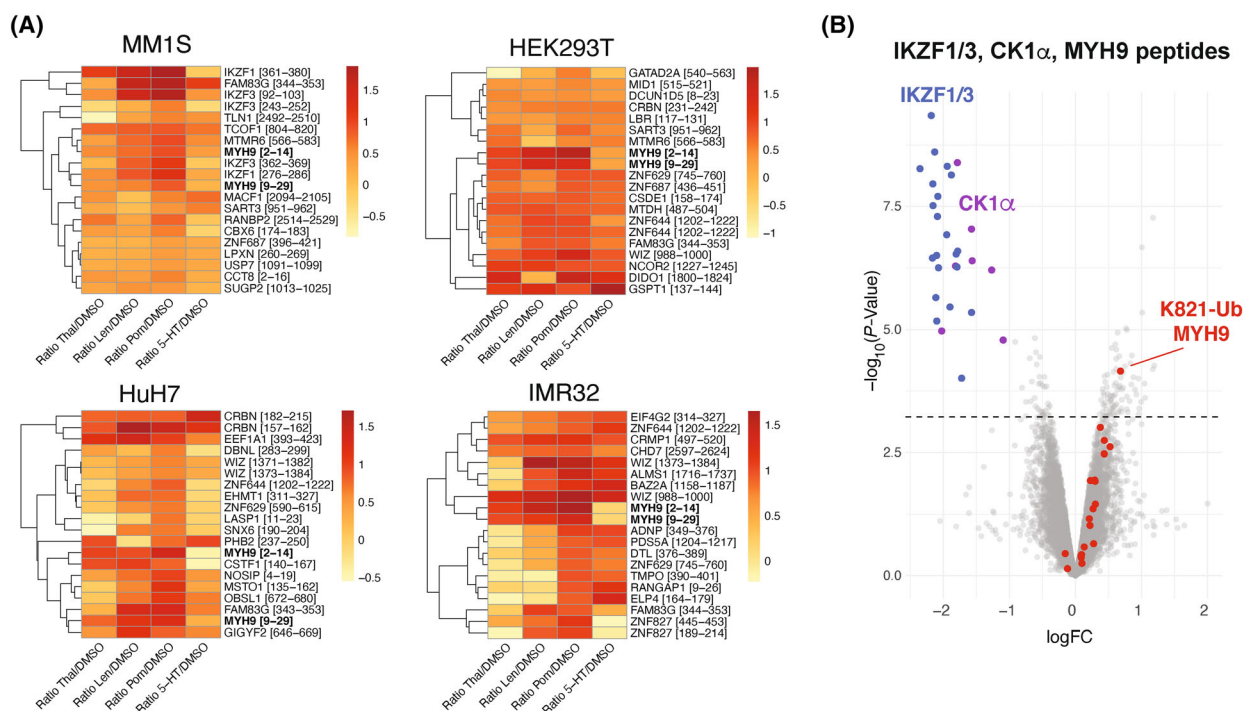


Fig. 6. Analysis of previously published MS data reveals that IMiDs causes CRBN-MYH9 interaction, and that Len induces ubiquitination of MYH9. (A) Heatmaps generated from publicly available data in the work of Yamanaka *et al.* [24]. These heatmaps show the top 20 peptides with highest biotinylation by AirlID-CRBN in MM.1S, HEK293T, HuH7, and IMR32 cells following treatment with thalidomide (Thal), lenalidomide (Len), pomalidomide (Pom) and the thalidomide metabolite 5-Hydroxythalidomide (5-HT). Peptides were filtered based on IMiD/DMSO ratio values > 0 that was significant for P -value < 0.05 in at least one of the four IMiD/DMSO ratios. The heatmap was generated with \log_{10} transformation of the ratios. Values between square brackets indicates the amino acid position of peptides in the protein of reference. MYH9 peptides are highlighted in bold characters. (B) Volcano plot, generated from publicly available data in the work of Krönke *et al.* [8]. This plot displays peptides containing ubiquitinated lysine in MM.1S cells treated with Len as compared to cells treated with DMSO. Blue dots represent ubiquitinated IKZF1 and IKZF3 peptides, violet dots represent ubiquitinated CK1 α peptides, red dots represent ubiquitinated MYH9 peptides. The dashed line sets the P -value cut-off that corresponds to the P -value of the peptide with the largest adj. P -value that is < 0.05 (adj. P -value = 0.04971141).

at 4 °C in 4 L of PBS (Gibco). PBS was changed twice a day. After 72 h, dialysed FBS was filter-sterilised through a 0.22 μ m filter and stored at -20 °C.

Compounds

Lenalidomide (cat #S1029), Pomalidomide (cat #S1567) and Ikerdomide (cat #S8760) were purchased from Selleckchem (Texas, USA). Bortezomib was kindly provided from excess clinical stocks by the Peter MacCallum Cancer Centre (Melbourne, Victoria, Australia) and Monash Health pharmacies (Clayton, Victoria, Australia).

Gibson assembly of CRBN open reading frame into *pBABE-mycBioID2-puroR*

A vector expressing myc-tagged-BioID2, *pBABE-mycBioID2-puroR*, was purchased from Addgene (cat. #80900, Watertown, MA, USA). The CRBN open reading

frame (ORF) was derived from the human CRBN transcript variant 2 (Table 1) and purchased from Biomatik (Kitchener, Ontario, Canada). The *pBABE-mycBioID2-puroR* was linearised via polymerase chain reaction (PCR) with Primer 1 and 2 (Table 1) using KAPA HiFi HotStart ReadyMix (cat #KK2601; Roche, Basel, Switzerland) as per manufacturer's instruction with the primers in Table 1. After linearising the vector, the CRBN open reading frame was amplified via PCR with Primer 3 and 4 (Table 1) using KAPA HiFi HotStart ReadyMix as per manufacturer's instruction. Subsequently, Gibson Assembly was performed between and CRBN ORF *pBABE-mycBioID2-puroR* with and with the NEBuilder HiFi DNA assembly Master Mix (cat #E2621, NEB - New England Biolabs, Ipswich, MA, USA) as per manufacturer's instructions using the PCR products obtained from the above reactions at a 1 : 5 vector to insert molar ratio. The assembled vector was validated via Sanger sequencing.

Table 1. Sequences and primers utilised for Gibson assembly of CRBN ORF and primers utilised to generate *pBABE-BiolD2-CRBN-puroR*.

| | Sequence |
|---|---|
| CRBN open reading frame (ORF) | ATGGCCGGCGAAGGAGATCAGCAGGACGCTGCGCACAACATGGGC AACCACCTGCCGCTCCTGCCTGAGAGTGAGGAAGAAGATGAAATGGAA GTTGAAGACCAGGATAGTAAAGAAGCCAAAAACCAACATCATAAA TTTTGACACTAGTCTGCCGACATCACATACATACCTAGGTGCTGATA TGGAAGAATTTCATGGCAGGACTTTGCACGATGACGACAGCTGTCA GGTGATTCCAGTTCTTCACAAGTGATGATGATCCTGATTCCCGGTCA GACATTACCTCTTCAGCTTTTTTACCCTCAAGAAGTCAGTA TGGTGCGGAATTTAATTCAGAAAGATAGAACCTTTGCTGTTCTTGCA TACAGCAATGTACAGGAAAGGGAAGCACAGTTTGGAAACAACAGCAGA GATATATGCCTATCGAGAAGAACAGGATTTTGGAAATTGAGATA GTGAAAGTGAAAGCAATTGGAAGACAAAGGTTCAAAGTACTTGA GCTAAGAACACAGTCAGATGGAATCCAGCAAGCTAAAGTGCAAA TTCTTCCCGAATGTGTGTTGCCTTCAACCATGTCTGCAGTTCAATTA GAATCCCTCAATAAGTGCCAGATATTTCTTCAAACCTGTCTCAAGA GAAGACCAATGTTTCATATAAGTGGTGGCAGAAATACCAGAAGAGAAA GTTTCATTGTGCAAATCTAACTTCATGGCCTCGCTGGCTGTA TTCCTTATATGATGCTGAGACCTTAATGGACAGAATCAAGAAACA GCTACGTGAATGGGATGAAAATCTAAAAGATGATTCTCTTCTTCAAA TCCAATAGATTTTTCTTACAGAGTAGCTGCTTGTCTTCTTATTGATGA TGTATTGAGAATTCAGCTCCTTAAATTTGGCAGTGCATCCAGCGA CTTCGCTGTGAATTAGACATTATGAATAAATGTA CTTCCCTTTGCTGTAAACAATGTCAAGAAACAGAAATAACAA CCAAAAATGAAATATTCAGTTTATCCTTATGTGGCCGATGGCA GCTTATGTGAATCCTCATGGATATGTGCATGAGACCTTACTGTGTA TAAGGCTTGCAACTTGAATCTGATAGGCCGGCCTTCTACAGAACACA GCTGGTTTTCTGGGTATGCCTGGACTGTTGCCAGTGTAAGA TCTGTGCAAGCCATATTGGATGGAAGTTTACGGCCACCAAAAAAGACA TGTCACCTCAAAAATTTGGGGCTTAACGCGATCTGCTCTGTTGCCCA CGATCCCAGACACTGAAGATGAAATAAGTCCAGACAAAGTAATA CTTTGCTTGTA CTCGAGTGACTTAAGTTTAAACCG |
| Primer 1: Forward primer for pBABE-mycBiolD2-puroR linearisation | |
| Primer 2: Reverse primer for pBABE-mycBiolD2-puroR linearisation | ACCACCACCGCTTCTTCTCAGGCTGAACTCTG |
| Primer 3: Forward primer for amplification of CRBN ORF with overhangs for Gibson assembly | AGTTCAGCCTGAGAAGAAGCGGTGGTGGTGCCGGCGAAGGAGATCAGC |
| Primer 4: Reverse primer for amplification of CRBN ORF with overhangs for Gibson assembly | TTTAAACTTAAGTCACTCGAGTTACAAGCAAAGTATTA |

Retroviral transduction

On day 0, 10 × 10⁶ HEK293T cells were plated 24 h prior to transfection in a T175 flask (CELLSTAR, Greiner Bio-One, Kremsmunster, Austria). On day 1, 30 µg of retroviral packaging vector, *pCL-Ampho* (cat #NBP2-29541; Novus Biologicals, Centennial, CO, USA), and 30 µg of target DNA were resuspended in DMEM (up to 1 mL) with no supplements. Polyethylenimine (PEI, 9002-98-6; Sigma-Aldrich, St Louis, MI, USA) was added to the mix at a 3 : 1 PEI : DNA ratio. Following addition of plasmids and PEI in medium, the solution was thoroughly vortexed and incubated at room temperature for 10 min. Finally, the DNA-PEI mix in DMEM was pipetted dropwise in the flask with growing HEK293T cells. On day 2, supernatant was discarded and replaced with fresh

DMEM with supplements (as previously described in the section ‘Cell lines and cell culture media’). On day 3, supernatant was collected, concentrated using concentrating columns (Amicon Ultra 15 mL Centrifugal Filters, cat #UFC903024; Merck Millipore, Burlington, MA, USA) replaced with fresh OPM2 cell media and filtered with a 0.45 µm strainer (Greiner Bio-One). Target cells were then plated at 100 000 mL⁻¹ in a 6-well plate (CELLSTAR, Greiner Bio-One) and cultured with collected medium containing lentiviral particles. 4 µg·mL⁻¹ Sequabrene (S2667; Sigma-Aldrich) was added to each well. On day 5, cells were harvested, washed and replated with fresh viral medium (with sequabrene 4 µg·mL⁻¹) for a second transduction hit. On day 6, cells were washed and re-plated with fresh medium.

Table 2. List of WB antibodies.

| Name | Species | Dilution | Manufacturer | Catalogue no. |
|-----------------------------|---------|------------|-------------------------------------|---------------|
| Anti-alpha-tubulin | Mouse | 1 : 10 000 | Sigma-Aldrich | T5168 |
| Anti-pan-Actin | Mouse | 1 : 10 000 | Invitrogen (Waltham, MA, USA) | MA5-11869 |
| Anti-CRBN | Rabbit | 1 : 1000 | Celgene corp (Summit, NJ, USA) | NA |
| Anti-MYH9 | Rabbit | 1 : 1000 | Abcam (Cambridge, UK) | ab238131 |
| Anti-myctag | Mouse | 1 : 1000 | CST (Danvers, MA, USA) | 2276 |
| Anti-Mouse-IgG HRP | Swine | 1 : 5000 | Agilent Dako (Santa Clara, CA, USA) | P0260 |
| Anti-Rabbit IgG HRP | Goat | 1 : 5000 | Agilent Dako | P0217 |
| Anti-Mouse Alexa Fluor 680 | Goat | 1 : 10 000 | Invitrogen | A28183 |
| Anti-Rabbit Alexa Fluor 800 | Goat | 1 : 10 000 | Invitrogen | A32735 |

Western blotting antibodies

All the antibodies utilised in western blotting analysis are listed in Table 2.

Quantification of sample protein concentration

Pierce BCA (Bicinchoninic Acid) Protein Assay Kit (23225; ThermoFisher Scientific) was employed for sample protein quantification. Serial dilution (2, 1, 0.5, 0.25, 0.125, 0.0625 and 0 mg·mL⁻¹) of Bovine Serum Albumin (BSA) within the kit in ultrapure dH₂O (NEB) were used as a standard reference for quantification of samples. Quantification solution (BCA + buffer) was made according to the manufacturer's instruction. In a 96-well plate, 190 µL of quantification solution was added to either 10 µL of each standard or 10 µL of each sample (diluted 1 : 10). A Spectramax iD3 plate reader (Molecular Devices, San Jose, CA, USA) was employed for measurement of absorbance ($\lambda = 565$ nm) in each sample to determine protein concentration.

Western blotting

Twenty to forty micrograms of protein (in 4× NuPAGE LDS sample buffer plus 10× NuPAGE Reducing Agent; Invitrogen) was loaded into 10-well or

12-well precast 4–12% gradient Bis-Tris NuPAGE gels (Invitrogen) for protein electrophoresis. Protein separation in was performed by electrophoresis at 120–160 V in Running Buffer (14.4 g Glycine, 3 g Tris base, 1 g SDS, in 1 L MilliQ water) for 120–150 min. Invitrogen PageRuler Plus Protein Ladder (Invitrogen) and Spectra Multicolor High Range Protein Ladder (Invitrogen) were used as protein molecular weight references. Proteins were transferred from gels to PVDF membranes (Immobilon-F; Merck Millipore) via semi-dry or wet transfer. Following transfer, membranes were blocked for 1 h in blocking buffer (5% w/v skim milk powder in TBS-Tween) or Intercept Odyssey buffer (LICOR, Lincoln, Nebraska, USA), washed with TBS-Tween and incubated overnight at 4 °C with a primary antibody (diluted with 5% BSA in TBS-Tween or in Intercept Odyssey buffer). The following day, membranes were washed in TBS-Tween, incubated with an HRP-conjugated anti-mouse or anti-rabbit secondary antibody (diluted respectively with 5% w/v skim milk powder in TBS-Tween) or with an Alexa Fluor 800-conjugated anti-rabbit IgG secondary or with an Alexa Fluor 680-conjugated anti-mouse IgG1 diluted in Intercept Odyssey buffer (LICOR). After incubation, membranes were washed three times with TBS-Tween. Finally, membranes were probed for immunoreactive bands using an ECL reagent (Amersham ECL or ECL Prime; GE Healthcare, Chicago, IL, USA) and revealed by film exposure (Fujifilm Super RX; Fujifilm, Minato City, Tokyo, Japan) with an AGFA CP1000 developer or by detection of fluorescent signal with an Odyssey scanner (LICOR).

Immunofluorescence

Wells of 96-well fluorescent microscopy chamber plates (cat #89626; ibidi, Grafelfing, Munich, Germany) were coated with poly-L-lysine (cat #P4707-50mL; Sigma-Aldrich) for 30 min, then left to dry after poly-L-lysine removal. After that, 5×10^4 OPM2 cells per well were seeded and incubated overnight, in RPMI media, treated with DMSO or lenalidomide 10 µM in 5% CO₂ at 37 °C. The next day, media was removed and replaced with 4% PFA (cat #C004; ProSciTech, Thuringowa, Queensland, Australia) in water for 15 min to fix the cells, followed by a wash with cold PBS. Then, cells were blocked in blocking buffer (PBS, 0.1% Triton X-100, 2% BSA) for 1 h at room temperature. Subsequently, blocking buffer was discarded and the primary antibodies diluted in blocking buffer (1 : 100 anti-MYH9 mouse monoclonal – Protein-tech, Rosemont, IL, USA, cat #60233-1-Ig; 1 : 200 anti-Ikaros rabbit polyclonal – Santa Cruz Biotechnology, Dallas, TX, USA, cat #sc-13039) added to the wells. Cells were incubated at room temperature for an hour to allow antibody binding. After that, cells were washed with cold

PBS and secondary antibodies and DAPI, diluted in blocking buffer, added to the cells prior to incubation for 1 h at room temperature in the dark (1 : 1000 anti-mouse IgG AlexaFluor-488 – Invitrogen cat #A11001, 1 : 1000 anti-rabbit IgG AlexaFluor-594 – Invitrogen cat #A11012, 1 : 1000 5 mg·mL⁻¹ DAPI – Sigma-Aldrich cat #D9542-1MG). Then, cells were washed with cold PBS, covered with cold, filtered PBS and imaged on Nikon C1 Confocal (Nikon, Minato City, Tokyo, Japan) using ×100 oil objective (1.4 NA). Three random fields of view were imaged for each condition.

Analysis and visualisation of immunofluorescence imaging

On IMAGEJ (National Institute of Health, Bethesda, MD, USA), a threshold based on the combined DAPI, MYH9, and Ikaros fluorescence of the middle z-slice was created for each field of view. The binary image was used to generate regions of interest outlining each cell. For each individual cell with inaccurate outlines, the ROI was manually drawn. Mean fluorescent intensity (MFI) was calculated for each cell, subtracting a blank background reading, for either anti-MYH9 and anti-Ikaros staining. The average MFI was calculated for each condition. Then, the Lent-treated cells MFI was adjusted relatively to DMSO-treated MFI for each individual experiment, and a *t*-test was performed on the relative values. Superplots were created in GRAPHPAD PRISM (La Jolla, CA, USA) as described by Lord *et al.* [53].

Cell lysis for enrichment of biotinylated proteins in OPM2 cells

OPM2-BioID2, OPM2-BioID2-CRBN cells were expanded and cultured for 8 h in biotin-free RPMI-1640 with 10% dFBS in T75 flasks. Cells were then spun at 300 rcf and replated at the density of 15×10^6 per flask in 20 mL of biotin-free media. Each flask represented a single technical replicate. Each experiment was performed with five technical replicates per treatment condition. After overnight treatment with 50 µM biotin (Sigma-Aldrich) and DMSO, IMiDs, bortezomib or a combination of bortezomib/IMiDs, all technical replicates were harvested on ice, spun at 300 rcf, washed with ice-cold PBS twice and transferred in Eppendorf 1.5 mL tubes. Cells were spun again at 300 rcf and supernatant discarded. Then, cell pellets were resuspended in 500 µL of RIPA buffer and incubated at 4 °C rotating for 30 min. Subsequently, lysates were spun at 20 000 rcf, supernatant collected and quantified through a BCA assay. Equal amounts of protein (1 mg) each sample were taken for processing. After that, samples were either snap-frozen at –80 °C or prepared for purification of biotinylated proteins.

Cell lysis for enrichment of biotinylated proteins in HEK293T cells transfected with BioID2-CRBN

7×10^6 HEK293T cells each sample were seeded in a T75 flask each. The next day, cells were transiently transfected with pBABE-BioID2-CRBN-puroR using 15 µg of DNA and 90 µg of polyethylenimine (PEI). On the following day, cells were harvested, pooled together, spun at 300 rcf and washed with PBS twice to remove biotin-containing medium. Cells were then split in 4 equal parts and reseeded in new T75 flasks in biotin-free DMEM (with GlutaMAX) Biotin-free DMEM was prepared by adding to DMEM + GlutaMAX dialysed FBS (dFBS) at a final concentration of 10%. The next day, treatments (biotin, DMSO and IMiDs) were added for 16 h. Cells were harvested the following day by centrifugation and washed with PBS twice to obtain pellet without residual cell culture media. Cells were lysed in 1 mL RIPA buffer (150 mM NaCl, 50 mM Tris pH 7.4, 0.1% SDS, 0.5% Sodium Deoxycholate, 1% Nonidet P-40, ddH₂O) with addition of protease inhibitors (cOmplete protease inhibitor cocktail, cat #11697498001; Roche) and incubated at 4 °C rotating for 30 min. Subsequently, lysates were spun at 20 000 rcf, supernatant collected and quantified through a BCA assay. Equal amounts of protein (1.7 mg) each sample were taken for processing. After that, samples were either snap-frozen at –80 °C or prepared for purification of biotinylated proteins.

Purification of biotinylated proteins for mass spectrometry

Ten microlitre of High-Capacity Streptavidin-Agarose resins (in 50% slurry, cat #20357; Pierce, Thermo-Fisher) per sample were used. Resins were initially spun at 2000 rcf for 1 min washed with 400 µL of RIPA buffer twice. Thus, 5 µL of beads were resuspended in each sample prior to incubation for 30–45 min at 4 °C rotating. Resins were spun at 2000 rcf, supernatant discarded and resins washed with 400 µL of RIPA buffer (×2, 4 °C). Then, resins were spun a 2000 rcf and washed with 400 µL of PBS-SDS (0.5% w/v SDS) at room temperature (×3), followed by incubation for 20 min with 100 µL of 100 mM dithiothreitol (DTT) SDS-PBS. Resins were subsequently washed with UC buffer (6 M urea, 100 mM Tris–HCl pH 8.5 in ddH₂O) twice in Spin-Cap columns (69725; Pierce). After that, samples were incubated with 100 µL UC buffer with 50 mM iodoacetamide in the dark for 20 min prior to several washing steps (400 µL UC buffer – six washes, 400 µL PBS – four washes, 400 µL ddH₂O – three washes). Protein immobilised in resins were digested overnight at 37 °C in 100 µL 50 mM NH₄HCO₃ (AMBIC) containing 2 µg of Trypsin Gold (cat #V5280; Promega, Madison, WI, USA). The next day, peptides were centrifuged at 1000 rcf for 1 min in Eppendorf Protein LoBind® 1.5 mL tubes

(0030108116; Eppendorf, Hamburg, Germany), resins washed again in 50 μ L of 50 mM AMBIC and acidified with 1% formic acid (FA) prior to freeze-dry and lyophilisation.

Purification of biotinylated proteins for western blotting

Forty microlitre of High-Capacity Streptavidin-Agarose resins (in 50% slurry, Pierce, Thermo-Fisher) per sample were used. Resins were initially spun at 2000 rcf for 1 min washed with 400 μ L of RIPA buffer four times. Following protein quantification with a BCA assay, 40 μ g of protein was collected as the whole cell lysate (input) fraction. Thus, 20 μ L of beads were resuspended in each of sample prior to incubation for 30–45 min at 4 °C rotating. Following incubation, resins were spun at 2000 rcf, supernatant discarded, and resins washed with 400 μ L of RIPA buffer (five times at 4 °C). After that, both input and enriched fraction were resuspended in sample buffer and boiled for 15 min at 95 °C. Forty micrograms of whole cell lysate and the purified fraction were loaded on an SDS/PAGE as described above (western blot paragraph).

Liquid chromatography–mass spectrometry (LC–MS/MS)

A M-class UPLC (Waters Corporation, Milford, MA, USA) coupled to a timsTOF Pro (Bruker, Bremen, Germany) with a CaptiveSpray source was employed for LC–MS/MS analysis. Peptides were lyophilised and subsequently resuspended in 1% formic acid (FA) plus 2% acetonitrile (ACN) and therefore separated on a 25 cm Aurora Series emitter column (25 cm \times 75 μ m, 1.6 μ m C18; IonOpticks, Fitzroy, Victoria, Australia). An integrated column oven (Sonation GmbH, Biberach, Germany) was used to maintain the temperature of the column at 50 °C. The column was equilibrated with a volume corresponding to five columns prior to loading sample in 100% buffer A (0.1% FA in MilliQ water). Separation of samples was performed at 400 nL.min^{−1} by employing a linear gradient with serial increases in concentration of buffer B (0.1% FA in ACN). The timsTOF Pro was run in PASEF mode (Compass Hystar 5.0.36.0, Bruker).

Peptide database search of label-free quantitation MS data

MAXQUANT 1.6.17 (Max Planck Institute of Biochemistry, Planegg, Germany) was adopted to process MS raw files. Common proteomics contaminants specific for trypsin digestion were allowed, with a maximum of two missed cleavages, when running the peptide search within the

Homo sapiens database. The minimum peptide length as criteria for inclusion in the search function was seven amino acids. Cysteine carbamidomethylation was set as fixed peptide modification. Protein N-terminal domains N-acetylation and methionine oxidation of were set as variable peptide modifications. A precursor ion mass error tolerance was set to 6 p.p.m. when performing the main search. A target-decoy approach was adopted to filter PSM and protein identifications at a false discovery rate (FDR) of 1% with use of match-between-runs.

Statistical analysis of label-free quantitation MS data

The output file proteinGroups.txt from MAXQUANT was used for further data processing and analysis on a customised pipeline developed in R. The peptide sequence, together with its charge and modification, was defined as a feature. Features not found in at least 50% of the replicates in one group were discarded. Volume variability was corrected by normalisation following log₂ transformation of the intensity of each feature. Log₂ intensity values were normalised by multiplying each value with the ratio of maximum median intensity of all replicates over median replicate intensity. Intensity values were imputed when missing to avoid infinite log₂(fold-change) using a randomly generated normal distribution of values. This distribution was generated with the following parameters: mean = mean_(intensities distribution) − 1.8 standard deviations (stdev), stdev = 0.3 \times stdev_(intensities distribution). The Limma R package was employed for differential protein enrichment between different treatment conditions and probability was corrected with Benjamini–Hochberg false discovery ratio (FDR).

Peptide database search of SILAC data (K-ε-GG dataset)

Raw ubiquitin-MS data from the work of Krönke *et al.* [8] was downloaded from the MassIVE repository (project ID MSV000079017). Raw MS data from replicate (triplicate) analyses were analysed with the MAXQUANT software version v2.1.3.0 and searched against the human Uniprot database (version 2022.09.20) and contaminants provided by the MAXQUANT software package. The search parameters were as follows: enzyme specificity was set to trypsin/P, maximum number of mixed cleavages set to 2, precursor mass tolerance was at 20 p.p.m. for the first search, and set to 4.5 p.p.m. for the main search. Oxidised methionines and N-terminal protein acetylation were searched as variable modifications, with carbamidomethylation of cysteines searched as a fixed modification. Gly-Gly addition to lysines was also searched as a variable modification. The minimum peptide length was set to 6, and the false discovery rate for peptide, protein, and site identification was set

to 1%. For protein quantitation, the label minimum ratio count was set to 2 and quantitation was performed on unmodified peptides and peptides with acetylation, oxidation and Gly-Gly modifications. Normalised ratios were utilised for quantification.

Statistical analysis of SILAC data (K-ε-GG dataset)

A sample loading (SL) normalisation was first applied on the SILAC intensity data in the MAXQUANT output file GlyGly (K)Sites.txt and subsequently followed by an internal reference scaling (IRS)-like normalisation [54] to correct the batch effect from the three different replicates. The intensity average of each replicate in each of the three experiments was used as reference channels for IRS-like normalisation.

A follow-up normalisation of the trimmed mean of *M* values [55] from edgeR package [56] in R (R Core Team) was applied and differential abundance analysis was then performed as described above for the statistical analysis of label-free quantitation data.

Software

RSTUDIO 4.2 (Posit, Boston, MA, USA) was utilised for all proteomics statistical analysis. STRING-db [57] was adopted for generation of protein–protein interaction networks, BIO-VEEN [58] was used for generation of Venn diagrams and TOPPFUN [59] was used for gene ontology analysis. IMAGEJ was adopted for processing of microscopy images.

Acknowledgements

We acknowledge funding for myeloma research from the Family of Mr Laurence Bode and a Monash Haematology Research Grant. JS is supported by an Australian NHMRC Fellowship (GNT2009177). We thank the Proteomics Facility at WEHI for providing expertise and equipment for the BioID2 proteomics screens. Open access publishing facilitated by Monash University, as part of the Wiley - Monash University agreement via the Council of Australian University Librarians.

Conflict of interest

The authors declare no conflict of interest. JS has received research funding from Amgen, Astex and Bristol Myers Squibb (BMS), speaker's honoraria from Novartis and Mundipharma and has served on advisory boards for Astellas, BMS, Pfizer and Otsuka. The Johnstone laboratory receives research funding from BMS and Pfizer. RWJ serves on the advisory Board of MycRx and is a shareholder in MycRx.

Author contributions

MC planned the project, conducted experimental work, analysed the data and wrote the manuscript. JJS provided technical assistance, performed proteomics experiments, and analysed the raw data of the BioID2 functional screens. BM and OS conducted experimental work. SJV contributed to project planning and provided supervision. JRD provided expertise for experimental work. DG, MRC, JRS, HVK and DG all contributed to the re-analysis of the publicly available ubiquitin-proteomics dataset. RWJ and JS planned the project, provided supervision, data interpretation, and wrote the manuscript.

Peer review

The peer review history for this article is available at <https://www.webofscience.com/api/gateway/wos/peer-review/10.1111/febs.17196>.

Data availability statement

The mass spectrometry proteomics data have been deposited to the ProteomeXchange Consortium via the PRIDE partner repository with the dataset identifier PXD050142.

References

- 1 Kumar SK, Rajkumar SV, Dispenzieri A, Lacy MQ, Hayman SR, Buadi FK, Zeldenrust SR, Dingli D, Russell SJ, Lust JA *et al.* (2008) Improved survival in multiple myeloma and the impact of novel therapies. *Blood* **111**, 2516–2520.
- 2 Gooding S, Ansari-Pour N, Towfic F, Estévez MO, Chamberlain PP, Tsai KT, Flynt E, Hirst M, Rozelle D, Dhiman P *et al.* (2021) Multiple cereblon genetic changes are associated with acquired resistance to lenalidomide or pomalidomide in multiple myeloma. *Blood* **137**, 232–237.
- 3 Kortüm KM, Mai EK, Hanafiah NH, Shi C-X, Zhu Y-X, Bruins L, Barrio S, Jedlowski P, Merz M *et al.* (2016) Targeted sequencing of refractory myeloma reveals a high incidence of mutations in CRBN and Ras pathway genes. *Blood* **128**, 1226–1233.
- 4 Ghobrial IM & Rajkumar SV (2003) Management of thalidomide toxicity. *J Support Oncol* **1**, 194–205.
- 5 Mateos M-V, García-Sanz R, Colado E, Olazábal J & San-Miguel J (2008) Should prophylactic granulocyte-colony stimulating factor be used in multiple myeloma patients developing neutropenia under lenalidomide-based therapy? *Br J Haematol* **140**, 324–326.

- 6 Palumbo A, Falco P, Corradini P, Falcone A, Di Raimondo F, Giuliani N, Crippa C, Ciccone G, Omedè P, Ambrosini MT *et al.* (2007) Melphalan, prednisone, and lenalidomide treatment for newly diagnosed myeloma: a report from the GIMEMA—Italian Multiple Myeloma Network. *J Clin Oncol* **25**, 4459–4465.
- 7 Hirsh J (2007) Risk of thrombosis with lenalidomide and its prevention with aspirin. *Chest* **131**, 275–277.
- 8 Krönke J, Udeshi ND, Narla A, Grauman P, Hurst SN, McConkey M, Svinkina T, Heckl D, Comer E, Li X *et al.* (2014) Lenalidomide causes selective degradation of IKZF1 and IKZF3 in multiple myeloma cells. *Science* **343**, 301–305.
- 9 Lu G, Middleton RE, Sun H, Naniong M, Ott CJ, Mitsiades CS, Wong K-K, Bradner JE & Kaelin WG (2014) The myeloma drug Lenalidomide promotes the cereblon-dependent destruction of Ikaros proteins. *Science* **343**, 305–309.
- 10 Sievers QL, Gasser JA, Cowley GS, Fischer ES & Ebert BL (2018) Genome-wide screen identifies cullin-RING ligase machinery required for lenalidomide-dependent CRL4CRBN activity. *Blood* **132**, 1293–1303.
- 11 Liu J, Song T, Zhou W, Xing L, Wang S, Ho M, Peng Z, Tai Y-T, Hideshima T, Anderson KC *et al.* (2019) A genome-scale CRISPR-Cas9 screening in myeloma cells identifies regulators of immunomodulatory drug sensitivity. *Leukemia* **33**, 171–180.
- 12 Chen Y-A, Peng Y-J, Hu M-C, Huang J-J, Chien Y-C, Wu J-T, Chen T-Y & Tang C-Y (2015) The Cullin 4A/B-DDB1-cereblon E3 ubiquitin ligase complex mediates the degradation of CLC-1 chloride channels. *Sci Rep* **5**, 10667.
- 13 Tateno S, Iida M, Fujii S, Suwa T, Katayama M, Tokuyama H, Yamamoto J, Ito T, Sakamoto S, Handa H *et al.* (2020) Genome-wide screening reveals a role for subcellular localization of CRBN in the anti-myeloma activity of pomalidomide. *Sci Rep* **10**, 4012.
- 14 Costacurta M, Vervoort SJ, Hogg SJ, Martin BP, Johnstone RW & Shortt J (2021) Whole genome CRISPR screening identifies TOP2B as a potential target for IMiD sensitization in multiple myeloma. *Haematologica* **106**, 2013–2017.
- 15 Van Nguyen T, Lee JE, Sweredoski MJ, Yang SJ, Jeon S-J, Harrison JS, Yim J-H, Lee SG, Handa H, Kuhlman B *et al.* (2016) Glutamine triggers acetylation-dependent degradation of glutamine synthetase via the thalidomide receptor cereblon. *Mol Cell* **61**, 809–820.
- 16 Lu G, Weng S, Matyskiela M, Zheng X, Fang W, Wood S, Surka C, Mizukoshi R, Lu C-C, Mendy D *et al.* (2018) UBE2G1 governs the destruction of cereblon neomorphic substrates. *Elife* **7**, e40958.
- 17 Sebastian S, Zhu YX, Braggio E, Shi C-X, Panchabhai SC, Van Wier SA, Ahmann GJ, Chesi M, Bergsagel PL, Stewart AK *et al.* (2017) Multiple myeloma cells' capacity to decompose H₂O₂ determines lenalidomide sensitivity. *Blood* **129**, 991–1007.
- 18 Eichner R, Heider M, Fernández-Sáiz V, van Bebber F, Garz A-K, Lemeer S, Rudelius M, Targosz B-S, Jacobs L, Knorn A-M *et al.* (2016) Immunomodulatory drugs disrupt the cereblon-CD147-MCT1 axis to exert antitumor activity and teratogenicity. *Nat Med* **22**, 735–743.
- 19 Heider M, Eichner R, Stroh J, Morath V, Kuisl A, Zecha J, Lawatscheck J, Baek K, Garz A-K, Rudelius M *et al.* (2021) The IMiD target CRBN determines HSP90 activity toward transmembrane proteins essential in multiple myeloma. *Mol Cell* **81**, 1170–1186.e10.
- 20 Costacurta M, He J, Thompson PE & Shortt J (2021) Molecular mechanisms of cereblon-interacting small molecules in multiple myeloma therapy. *J Pers Med* **11**, 1185.
- 21 Roux KJ, Kim DI, Raida M & Burke B (2012) A promiscuous biotin ligase fusion protein identifies proximal and interacting proteins in mammalian cells. *J Cell Biol* **196**, 801–810.
- 22 Roux KJ, Kim DI, Burke B & May DG (2018) BioID: a screen for protein-protein interactions. *Curr Protoc Protein Sci* **91**, 19.23.1–19.23.15.
- 23 Kim DI, Jensen SC, Noble KA, Kc B, Roux KH, Motamedchaboki K & Roux KJ (2016) An improved smaller biotin ligase for BioID proximity labeling. *Mol Biol Cell* **27**, 1188–1196.
- 24 Yamanaka S, Horiuchi Y, Matsuoka S, Kido K, Nishino K, Maeno M, Shibata N, Kosako H & Sawasaki T (2022) A proximity biotinylation-based approach to identify protein-E3 ligase interactions induced by PROTACs and molecular glues. *Nat Commun* **13**, 183.
- 25 Pecci A, Ma X, Savoia A & Adelstein RS (2018) MYH9: structure, functions and role of non-muscle myosin IIA in human disease. *Gene* **664**, 152–167.
- 26 Asensio-Juárez G, Llorente-González C & Vicente-Manzanares M (2020) Linking the landscape of MYH9-related diseases to the molecular mechanisms that control non-muscle myosin II-A function in cells. *Cells* **9**, 1458.
- 27 Vicente-Manzanares M, Ma X, Adelstein RS & Horwitz AR (2009) Non-muscle myosin II takes centre stage in cell adhesion and migration. *Nat Rev Mol Cell Biol* **10**, 778–790.
- 28 Li X & Song Y (2020) Proteolysis-targeting chimera (PROTAC) for targeted protein degradation and cancer therapy. *J Hematol Oncol* **13**, 50.
- 29 Sievers QL, Petzold G, Bunker RD, Renneville A, Ślabcicki M, Liddicoat BJ, Abdulrahman W, Mikkelsen T, Ebert BL & Thomä NH (2018) Defining the human C2H2 zinc finger degrome targeted by thalidomide analogs through CRBN. *Science* **362**, eaat0572.
- 30 Dunbar K, Macartney TJ & Sapkota GP (2021) IMiDs induce FAM83F degradation via an interaction with

- CK1 α to attenuate Wnt signalling. *Life Sci Alliance* **4**, e202000804.
- 31 Krönke J, Fink EC, Hollenbach PW, MacBeth KJ, Hurst SN, Udeshi ND, Chamberlain PP, Mani DR, Man HW, Gandhi AK *et al.* (2015) Lenalidomide induces ubiquitination and degradation of CK1 α in del(5q) MDS. *Nature* **523**, 183–188.
 - 32 Lonial S, van de Donk NWCJ, Popat R, Zonder JA, Minnema MC, Larsen J, Nguyen TV, Chen MS, Bensmaine A, Cota M *et al.* (2019) First clinical (phase 1b/2a) study of iberdomide (CC-220; IBER), a CELMoD, in combination with dexamethasone (DEX) in patients (pts) with relapsed/refractory multiple myeloma (RRMM). *J Clin Oncol* **37** *suppl.*, 8006.
 - 33 Akber U, Jo H, Jeon S, Yang SJ, Bong S, Lim S, Kim YK, Park ZY & Park CS (2021) Cereblon regulates the proteotoxicity of tau by tuning the chaperone activity of DNAJA1. *J Neurosci* **41**, 5138–5156.
 - 34 Gano JJ & Simon JA (2010) A proteomic investigation of ligand-dependent HSP90 complexes reveals CHORDC1 as a novel ADP-dependent HSP90-interacting protein. *Mol Cell Proteomics* **9**, 255–270.
 - 35 Liu W, Lu Y, Yan X, Lu Q, Sun Y, Wan X, Li Y, Zhao J, Li Y & Jiang G (2022) Current understanding on the role of CCT3 in cancer research. *Front Oncol* **12**, 961733.
 - 36 Fournier MJ, Gareau C & Mazroui R (2010) The chemotherapeutic agent bortezomib induces the formation of stress granules. *Cancer Cell Int* **10**, 12.
 - 37 Marcelo A, Koppenol R, de Almeida LP, Matos CA & Nóbrega C (2021) Stress granules, RNA-binding proteins and polyglutamine diseases: too much aggregation? *Cell Death Dis* **12**, 592.
 - 38 Mazroui R, Di Marco S, Kaufman RJ & Gallouzi I-E (2007) Inhibition of the ubiquitin-proteasome system induces stress granule formation. *Mol Biol Cell* **18**, 2603–2618.
 - 39 Fischer ES, Böhm K, Lydeard JR, Yang H, Stadler MB, Cavadini S, Nagel J, Serluca F, Acker V, Lingaraju GM *et al.* (2014) Structure of the DDB1–CRBN E3 ubiquitin ligase in complex with thalidomide. *Nature* **512**, 49–53.
 - 40 Liu J, Liu Z, Yan W, Yang H, Fang S, Deng S, Wen Y, Shen P, Li Y, Hou R *et al.* (2022) ENKUR recruits FBXW7 to ubiquitinate and degrade MYH9 and further suppress MYH9-induced deubiquitination of β -catenin to block gastric cancer metastasis. *MedComm* **3**, e185.
 - 41 Yamamoto Y, Chino H, Tsukamoto S, Ode KL, Ueda HR & Mizushima N (2021) NEK9 regulates primary cilia formation by acting as a selective autophagy adaptor for MYH9/myosin IIA. *Nat Commun* **12**, 3292.
 - 42 Ye Y & Rape M (2009) Building ubiquitin chains: E2 enzymes at work. *Nat Rev Mol Cell Biol* **10**, 755–764.
 - 43 Althaus K & Greinacher A (2009) MYH9-related platelet disorders. *Semin Thromb Hemost* **35**, 189–203.
 - 44 Kelley MJ, Jawien W, Ortel TL & Korczak JF (2000) Mutation of MYH9, encoding non-muscle myosin heavy chain A, in May-Hegglin anomaly. *Nat Genet* **26**, 106–108.
 - 45 Kurochkina N & Guha U (2013) SH3 domains: modules of protein-protein interactions. *Biophys Rev* **5**, 29–39.
 - 46 Palumbo A, Rajkumar SV, Dimopoulos MA, Richardson PG, Miguel JS, Barlogie B, Harousseau J, Zonder JA, Cavo M, Zangari M *et al.* (2008) Prevention of thalidomide- and lenalidomide-associated thrombosis in myeloma. *Leukemia* **22**, 414–423.
 - 47 Girolamo A, Vettore S, Bonamigo E & Fabris F (2011) Thrombotic events in MYH9 gene-related autosomal macrothrombocytopenias (old May-Hegglin, Sebastian, Fechtner and Epstein syndromes). *J Thromb Thrombolysis* **32**, 474–477.
 - 48 Tochigi T, Miyamoto T, Hatakeyama K, Sakoda T, Ishihara D, Irifune H, Shima T, Kato K, Maeda T, Ito T *et al.* (2020) Aromatase is a novel neosubstrate of cereblon responsible for immunomodulatory drug-induced thrombocytopenia. *Blood* **135**, 2146–2158.
 - 49 Pal R, Monaghan SA, Hassett AC, Mapara MY, Schafer P, Roodman GD, Ragni MV, Moscinski L, List A & Lentzsch S (2010) Immunomodulatory derivatives induce PU.1 down-regulation, myeloid maturation arrest, and neutropenia. *Blood* **115**, 605–614.
 - 50 Xu Y, Li J, Ferguson GD, Mercurio F, Khambatta G, Morrison L, Lopez-Girona A, Corral LG, Webb DR, Bennett BL *et al.* (2009) Immunomodulatory drugs reorganize cytoskeleton by modulating rho GTPases. *Blood* **114**, 338–345.
 - 51 Fionda C, Stabile H, Molfetta R, Kosta A, Peruzzi G, Ruggeri S, Zingoni A, Capuano C, Soriani A, Paolini R *et al.* (2021) Cereblon regulates NK cell cytotoxicity and migration via Rac1 activation. *Eur J Immunol* **51**, 2607–2617.
 - 52 Lagrue K, Carisey A, Morgan DJ, Chopra R & Davis DM (2015) Lenalidomide augments actin remodeling and lowers NK-cell activation thresholds. *Blood* **126**, 50–60.
 - 53 Lord SJ, Velle KB, Dyche Mullins R & Fritz-Laylin LK (2020) SuperPlots: communicating reproducibility and variability in cell biology. *J Cell Biol* **219**, e202001064.
 - 54 Plubell DL, Wilmarth PA, Zhao Y, Fenton AM, Minnier J, Reddy AP, Klimek J, Yang X, David LL & Pamir N (2017) Extended multiplexing of tandem mass tags (TMT) labeling reveals age and high fat diet specific proteome changes in mouse epididymal adipose tissue. *Mol Cell Proteomics* **16**, 873–890.
 - 55 Robinson MD & Oshlack A (2010) A scaling normalization method for differential expression analysis of RNA-seq data. *Genome Biol* **11**, R25.

- 56 Robinson MD, McCarthy DJ & Smyth GK (2009) edgeR: a Bioconductor package for differential expression analysis of digital gene expression data. *Bioinformatics* **26**, 139–140.
- 57 Szklarczyk D, Franceschini A, Wyder S, Forslund K, Heller D, Huerta-Cepas J, Simonovic M, Roth A, Santos A, Tsafou KP *et al.* (2015) STRING v10: protein-protein interaction networks, integrated over the tree of life. *Nucleic Acids Res* **43**, D447–D452.
- 58 Hulsen T, de Vlieg J & Alkema W (2008) BioVenn – a web application for the comparison and visualization of biological lists using area-proportional Venn diagrams. *BMC Genomics* **9**, 488.
- 59 Chen J, Bardes EE, Aronow BJ & Jegga AG (2009) ToppGene suite for gene list enrichment analysis and candidate gene prioritization. *Nucleic Acids Res* **37**, W305–311.

Supporting information

Additional supporting information may be found online in the Supporting Information section at the end of the article.

Appendix S1. Supporting Information.